Ultrasonics Sonochemistry 73 (2021) 105501

Contents lists available at ScienceDirect

Ultrasonics Sonochemistry

journal homepage: www.elsevier.com/locate/ultson

New insights into the mechanisms of ultrasonic emulsification in the oil–water system and the role of gas bubbles

W.H. Wu [a], D.G. Eskin [b,c,*], A. Priyadarshi [d], T. Subroto [b], I. Tzanakis [d,e], W. Zhai [a,*]

[a] School of Physical Science and Technology, Northwestern Polytechnical University, Xi'an 710072, PR China
[b] Brunel Centre for Advanced Solidification Technology (BCAST), Brunel University London, Uxbridge UB8 3PH, United Kingdom
[c] Tomsk State University, Tomsk 634050, Russian Federation
[d] Faculty of Technology, Design and Environment, Oxford Brookes University, Oxford OX33 1HX, United Kingdom
[e] Department of Materials, University of Oxford, Oxford OX1 3PH, United Kingdom

ARTICLE INFO

Keywords:
Ultrasonic emulsification
Cavitation
Gas bubble
Oil-water
High-speed visualization

ABSTRACT

Ultrasonic emulsification (USE) assisted by cavitation is an effective method to produce emulsion droplets. However, the role of gas bubbles in the USE process still remains unclear. Hence, in the present paper, high-speed camera observations of bubble evolution and emulsion droplets formation in oil and water were used to capture in real-time the emulsification process, while experiments with different gas concentrations were carried out to investigate the effect of gas bubbles on droplet size. The results show that at the interface of oil and water, gas bubbles with a radius larger than the resonance radius collapse and sink into the water phase, inducing (oil–-water) blended liquid jets across bubbles to generate oil-in-water-in-oil (O/W/O) and water-in-oil (W/O) droplets in the oil phase and oil-in-water (O/W) droplets in the water phase, respectively. Gas bubbles with a radius smaller than the resonance radius at the interface always move towards the oil phase, accompanied with the generation of water droplets in the oil phase. In the oil phase, gas bubbles, which can attract bubbles nearby the interface, migrate to the interface of oil and water due to acoustic streaming, and generate numerous droplets. As for the gas bubbles in the water phase, those can break neighboring droplets into numerous finer ones during bubble oscillation. With the increase in gas content, more bubbles undergo chaotic oscillation, leading to smaller and more stable emulsion droplets, which explains the beneficial role of gas bubbles in USE. Violently oscillating microbubbles are, therefore, found to be the governing cavitation regime for emulsification process. These results provide new insights to the mechanisms of gas bubbles in oil–water emulsions, which may be useful towards the optimization of USE process in industry.

1. Introduction

Emulsion is composed of at least two immiscible liquids, in which the dispersed phase is distributed in the continuous phase in the form of small droplets [1–3]. As an important vehicle for transporting bioactive materials, emulsion is widely applied in the food and pharmaceutical industries [4,5]. For example, stable oil-in-water (O/W) type emulsions can efficiently deliver oil-soluble components into foods [6]. The keys to generate stable droplets in the continuous phase are high energy shear, mixing and turbulence [7]. Nowadays, there are many methods to prepare emulsion, such as rotor–stator type devices, high-pressure homogenization (HPH), microfluidization (MF) and ultrasonic emulsification (USE) [8,9]. Comparing with other techniques, USE possesses many advantages, such as high energy efficiency, small droplet size and easy operation [10].

The classical model of USE process, which was suggested by Neduzhii [11] in 1964 and then developed further by Fogler and Li [12,13] in 1978, comprises two stages. In the first stage, ultrasound introduced into the liquid induces a wave-like instability of an interface, e.g. oil–water, leading to the eruption of the dispersed phase into the continuous phase as large droplets. In the second stage, the physical effects generated by cavitation near the interface, including micro jets, high-pressure shock waves up to 1 GPa and high local shear forces [14–17], break large droplets into small ones. With continuous sonication, the droplet size gradually reduces to its limit.

However, recent research showed that USE process is much more

* Corresponding authors at: Brunel Centre for Advanced Solidification Technology (BCAST), Brunel University London, Uxbridge UB8 3PH, United Kingdom (D.G. Eskin) and School of Physical Science and Technology, Northwestern Polytechnical University, Xi'an 710072, PR China (W. Zhai).
E-mail addresses: dmitry.eskin@brunel.ac.uk (D.G. Eskin), zhaiwei322@nwpu.edu.cn (W. Zhai).

https://doi.org/10.1016/j.ultsonch.2021.105501
Received 8 December 2020; Received in revised form 31 January 2021; Accepted 17 February 2021
Available online 23 February 2021

complex than just these two stages. Perdih et al. [18] carried out in-situ observations to study the mechanism for O/W emulsion prepared by ultrasonic processing. They found that besides the above two stages, there were additional intermediate steps to produce W/O and even O/W/O droplets by cavitation. In addition, Leong et al. [19] and Vankova et al. [20] indicated that the droplet breakup was primarily affected by eddies and shear stresses generated during bubble collapse. In most liquids, acoustic cavitation bubbles induced under continuous ultrasonic waves are actually filled with and dissolved in the liquid gases that prolong their lifetime and cavitation activity [21]. It is then logical to suggest that the concentration of the gas in the liquid as well as the amount of gas bubbles would affect the emulsification process. The reported results are, however, quite controversial. Behrend and Schubert [22] demonstrated that the mean droplet size was the function of the energy density, and no clear influence of gas content was observed on droplet disruption at a constant energy density. Nevertheless, Rooze et al. [23] concluded that gas and vapor determined the thermal properties of a cavitation bubble during collapse, and the addition of gas to the liquid lowered its surface tension, leading to the increase in cavitation bubble nucleation. On the other hand, a lower surface tension has been proven to suppress cavitation intensity due to the absence of major collapsing events and large bubble clusters [24]. Chen et al. [25] introduced N_2 into USE process and demonstrated the efficiency of this method in producing a stable temperature-responsive Pickering emulsion. These contradicting reports show that there is a clear gap in our knowledge about the effects of gas concentration on the bubble dynamics, and eventually, on the USE.

Oil and water are transparent before complete mix, so it is feasible to observe the real-time evolution of gas bubbles by a high-speed camera [26,27]. Orthaber et al. [28] studied the bubble movement near the oil–water interface by in-situ observation and numerical simulation. They found that the jet generated by bubble collapse always moved toward the interface if the bubble grew in the lighter liquid, and correspondingly away from the interface if it was initiated inside the denser liquid. Cucheval et al. [29] observed the emulsification process at the oil–water interface, and the results showed that an emulsion could only be obtained if the interface was within the cavitation zone. It can be seen that researchers have paid attention to the bubbles initially located at the oil–water interface, but there have been no reports on the role of bubbles located in the bulk of the oil and water phases.

In present work, we aim to clarify the mechanisms of gas bubbles in the USE process by using high-speed observations of the bubble dynamics in the oil phase, the water phase and at the interface. The resultant size distributions of droplets in the emulsions produced within distilled and carbonated water are quantified. According to the experimental results, new insights to the mechanisms of gas bubbles in emulsion preparation by ultrasound are provided.

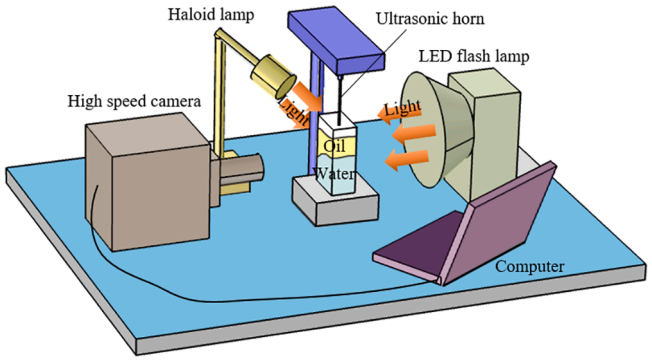

Fig. 1. Schematic diagram of experimental setup for in-situ observation.

2. Materials and methods

A schematic diagram of the experimental setup is shown in Fig. 1. The inner size of a transparent plastic container was 20 × 10 × 40 mm, and the wall thickness was 2.5 mm. There were 2 ml of water and 1 ml of sunflower oil in the container with a layer of oil on top of a layer of water. The total level of liquid in the container was 15 mm. The carbonated water (with gas concentration in the range 3–3.5 g/l), which can produce numerous gas bubbles during USE, was used so that the bubbles evolution in the water phase can be easily captured. Otherwise, distilled water (with gas concentration < 10 mg/l) was used to record bubbles evolution in the oil phase and at the interface of water and oil. A Ti sonotrode, 3 mm in diameter, coupled with a 200-W piezoelectric transducer (Hielscher) at a driving frequency of 24 kHz, was inserted into the oil phase 3 ~ 5 mm away from the oil–water interface. The peak-to-peak amplitudes were 84 μm when bubbles were at the interface, and 210 μm when bubbles were in the oil phase or in the water phase. In order to force bubbles to collapse and enable direct observations of the related effects, the maximum power (100% of transducer capacity) was used in the last two cases. Upon USE initiation, a high-speed camera (Photron Fastcam SA-Z) and a specialized LED illumination system (a 150-W AmScope Hl-250a Fiber Optic Illuminator Haloid Lamp in front and a GSVITEC MultiLED flash lamp from the back) were used to record the real-time process with an image acquisition rate of 100,000 frames per second (fps). Only the first milliseconds of the process have been observed before the developed cavitation zone formed under the sonotrode and reached the camera field of view, allowing clear and accurate observations of the behavior of gas bubbles under ultrasonic field. The obtained image sequences were analyzed and quantified manually.

After the in-situ observations of emulsification process, the effect of gas content on the size distribution of emulsion droplets was studied in a separate series of experiments. To obtain relatively uniform emulsion droplets, 2 ml of surfactant (Tween-80) was instilled into 2 ml of oil and 36 ml of water. Ultrasound was induced by a stainless-steel rectangular shape sonotrode, with a tip of 3 × 8 mm, coupled with an ultrasonic transducer (1800 W, 20 kHz, FS-1800 N). The sonotrode was inserted from the top of the initial oil layer. During USE, 40% ultrasonic power, corresponding to the 44-μm peak-to-peak amplitude was used to process the liquid mixture for 4 min. In these experiments, the same two water types, i.e. distilled water and commercial carbonated water, were used. After that, the generated O/W emulsion droplets were observed by an optical microscope (OLYMPUS-CKX41) and quantified by the software Nano Measurer 1.2.

It should be noted that the above two experiments were independent and aimed at observing the bubble dynamics and studying the effect of gas content on ultrasonic emulsification, respectively. Although the liquid volume, container shape and scale and ultrasonic device were different, they did not affect the targeted experimental phenomena and final conclusions.

3. Results and discussion

3.1. In-situ studies of USE mechanisms

3.1.1. A bubble in the oil phase at the interface of oil and water

Fig. 2 depicts a gas bubble with an initial radius of 573 μm located at the interface of oil and water. See online Video 1 for more detailed observations. When ultrasound is introduced into the oil, the bubble is subjected to a travelling ultrasonic wave, and experiences stable oscillations, as shown in Fig. 2(a) and (b). Meanwhile, the bubble gradually moves towards the interface, and the oil layers, i.e. the stretched areas of oil, are generated due to surface tension gradients from the oil source to the water, as shown in Fig. 2(c). At the next oscillation period (in Fig. 2 (d)), the bubble shrinks and attracts nearby liquids. Oil layers retract and become thinner, dragging some water to the bubble wall, which is

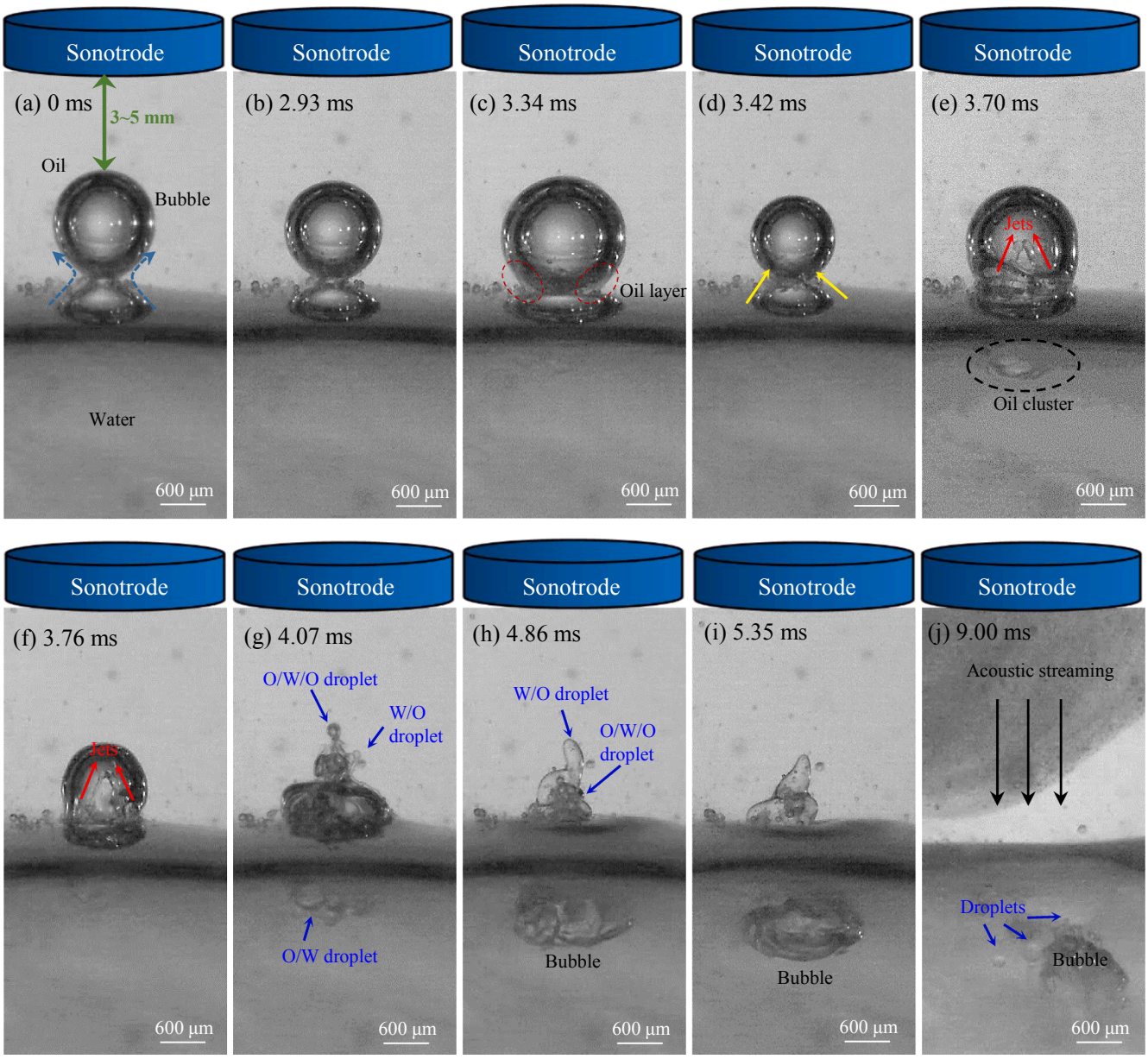

Fig. 2. Evolution of the bubble with an initial radius of 573 μm at the interface of oil and water. The supplementary video can be accessed with the online version of the article as Video 1.

now ready for the stage of emulsification. At 3.7 ms, the bubble gradually submerges into the water phase, accompanied with a layer of oil at the bubble wall, and a novel phenomenon is observed. Due to the strong contraction during bubble oscillations, there is a drastic perturbation at the interface. Oil and water at the bubble wall are sucked into the bubble, and generate two beams of blended liquid jets, that move upwards and towards the oil phase, travelling through the bubble wall with a speed of about 1.7 m/s (Fig. 2(e) and (f)). As a result, some opaque and transparent droplets (Fig. 2(g)-(h)) are produced in the oil phase, which are O/W/O droplets and W/O droplets, respectively, similar to those reported by Perdih et al. [18]. Meanwhile, the bubble collapse leads to complex turbulence typically composed of annular stagnation rings and secondary vortices [30], which promotes the mixing of oil and water, so there is an oil cluster formed in water as shown in Fig. 2(e). The cavitating bubble gradually moves into the water phase, and its continuous perturbation in the acoustic field makes the oil cluster split into numerous transparent O/W droplets, as presented in Fig. 2(g). At the end, acoustic streaming emitted from ultrasonic horn, arrives at the interface, and pushes all formed droplets into the water phase in Fig. 2 (j).

When there is a smaller bubble with an initial radius of 95 μm at the interface, a different bubble dynamic behavior is observed as presented in Fig. 3. At first, the bubble keeps a spherical oscillation. After that, instead of sinking into the water like the bigger bubble in Fig. 2, it moves upwards in the oil phase in a stable cavitating manner. There is an invert funnel-shaped hump formed at the interface beneath the gas bubble, and a small droplet is extracted from the water phase and rises up with a speed of about 0.3 m/s, as shown in Fig. 3(b)-(e). The whole process can be seen more clearly in online Video 2.

It can be seen from the aforementioned results that large size bubbles cavitate at the interface in a transient manner that can be referred to as high-energy stable cavitation [31] and then, upon vigorous surface deformation, violently penetrate into the water phase; while small size bubbles float into the oil phase and towards the cavitation area in a stable manner known as low-energy stable cavitation [31]. The reason may be that the motion direction of a gas bubble near a pressure

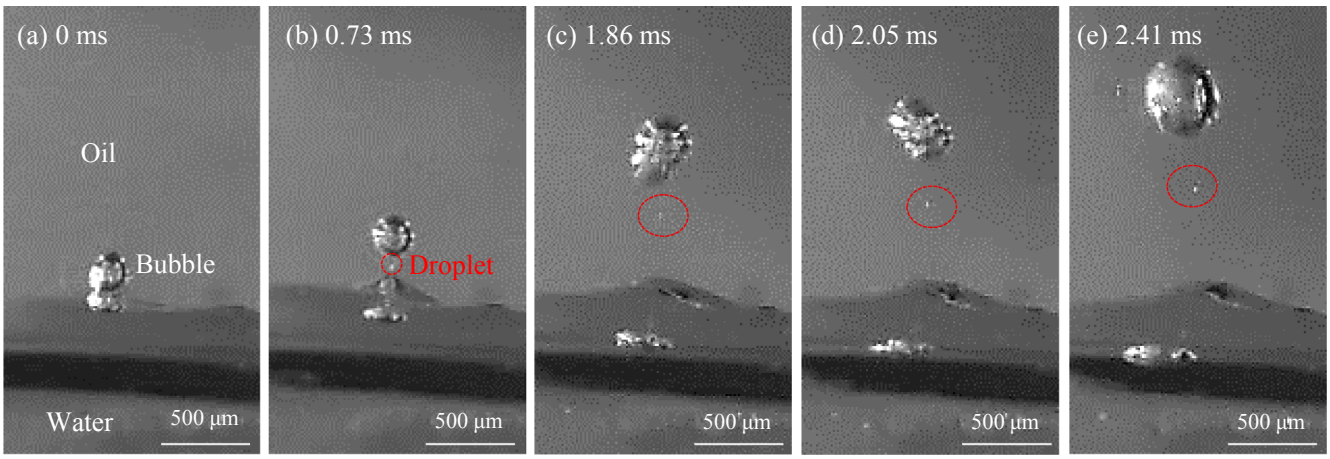

Fig. 3. In-situ observation of a small bubble with an initial radius of 95 μm at the interface: (a) 0 ms; (b) 0.73 ms; (c) 1.86 ms; (d) 2.05 ms; (e) 2.41 ms. The supplementary video can be accessed with the online version of the article as Video 2.

antinode depends on the primary Bjerknes force [32,33]. A bubble smaller than the resonance radius of a freely oscillating bubble is attracted to the pressure antinode, while a bubble larger than the resonance radius escapes from there. According to the Minnaert equation [33], the resonance radius R_{res} of a bubble in oil can be derived by:

$$f_r = \frac{1}{2\pi R_{res}}\sqrt{\frac{3\kappa P_0 + (3\kappa - 1)\frac{2\sigma}{R_{res}}}{\rho_0}} \quad (1)$$

where f_r is the resonance frequency; ρ_0 and σ are the density and surface tension of oil, respectively; P_0 is the static pressure, and κ is the polytropic exponent. The physical parameters used in the calculation are listed in Table 1. It can be calculated from Eq. (1) that the resonance bubble radius R_{res} in the oil is 145 μm. We can expect a strong pressure antinode under the ultrasonic horn, which is located just 3.7 mm above the oil/water interface. Therefore, the bubble at the interface in Fig. 2 with a radius of 573 μm is larger than R_{res}, and its motion is controlled by the primary Bjerknes force, submerging it into the water phase. On the contrary, the bubble in Fig. 3 with a radius of 95 μm is smaller than R_{res}, and it moves towards the ultrasonic source inside the oil phase, picking small droplets from the disturbed (by the bubble cavitation) interface in its wake.

3.1.2. A bubble in the oil phase away from the interface

Fig. 4(a) depicts the situation when a gas bubble with an initial radius of 1.6 mm is located directly beneath the ultrasonic horn in the oil phase. When the horn starts to oscillate, the gas bubble inside the cavitation zone undergoes vigorous oscillations, grows into a bubbly cloud and rapidly collapses, producing multiple liquid jets that pierce and gradually split the bubble into numerous bubbles accompanied by chaotic oscillations and shape distortions, and the ejection of multiple smaller in size satellite bubbles (as shown in Fig. 4(d)-(f)). At this point it should be noted that with the term chaotic oscillation we refer to non-periodic violent shape bubble oscillations as previously defined in Refs. [33,36]. Supplementary Video 3 gives a clearer presentation of the above process. It can be seen from Fig. 4(f) that bubble A is pushed along the interface to the water phase by the liquid flow, dragging oil into the water phase to produce some small size droplets in the wake of the bubble. At the same time, the oil is continuously pushed into the water phase by acoustic streaming, with numerous droplets forming in the water phase. It is evident (see Video 3 for more detail) that the droplets in Area I in Fig. 4(g), where bubble A is located and chaotically oscillates, are smaller than those in Area II where there is no cavitation effect. In order to quantitatively analyze the droplet size of the two areas, the distribution of droplet diameters is given in Fig. 4(i). Due to the resolution limitation, only those droplets with recognizable spherical shape were counted. It can be found that the averaged diameters of droplets in Areas I and II are respectively 192 ± 90 and 321 ± 114 μm, which indicates that the presence of the primary cavitation/gas bubble in the oil phase can enhance the emulsification efficiency by disturbing the interface and by producing satellite bubbles of smaller size that further oscillate at the interface.

Fig. 5 depicts a situation when there are two bubbles of similar dimensions in the oil phase. Bubble B1 with an initial radius of 236 μm is located in the bulk of the oil phase, and bubble B2 with an initial radius of 264 μm is at the interface. Both bubbles have the radii larger than the resonance radius. According to the analysis in Section 3.1.1 (Fig. 2), bubble B2 should collapse and sink into the water phase. However, the existence of bubble B1 drives bubble B2 to float up. This is attributed to the secondary Bjerknes force generated by bubble B1, which can be calculated as follows [37]:

$$F_{1\to 2} = \frac{\rho_0}{4\pi L^2}\left\langle \ddot{V}_1 V_2 \right\rangle e_{1\to 2} \quad (2)$$

V_1 and V_2 are, respectively, the volumes of B1 and B2, and $\boldsymbol{e}_{1\to 2}$ is the unit vector directed from B1 to B2. If the coefficient of $\boldsymbol{e}_{1\to 2}$ is negative, the secondary Bjerknes force is attractive. L is the distance between the bubble centers of B1 and B2. When L decreases to a threshold value, the secondary Bjerknes force overcomes the primary Bjerknes force, which causes bubble B2 to rise up. Meanwhile, the oil/water interface is disturbed, forming a channel towards the rising bubble B2, and water beneath the channel is sucked into the bubble, leading to the generation of a jet similar to those in Fig. 2(b). The continuous drag force from bubble B2 attracts water and oil to gather in the narrow channel at 0.44 ms, thus forming numerous O/W droplets (shown in a like-lay eggs formation) with diameters of about 120 μm in the channel, as shown in Fig. 5(c) and (d). Note that when the developed cavitation zone from the sonotrode reaches bubble B1, the bubble starts to vigorously oscillate forming a characteristic "pancake shape" (Fig. 5(b)) and ejecting liquid jets [38] (seen as a cloud of tiny bubbles in the top part of Fig. 5(b) and

Table 1
Physical parameters used in calculation [34,35].

Parameter	Unit	Value
Density of oil ρ_0	kg/m^3	892
Surface tension of oil σ	N/m	0.033
Resonant frequency f_r	kHz	24
Static pressure p_0	Pa	101,325
Polytropic exponent κ	1	1.4
Interfacial tension γ	N/m	0.025

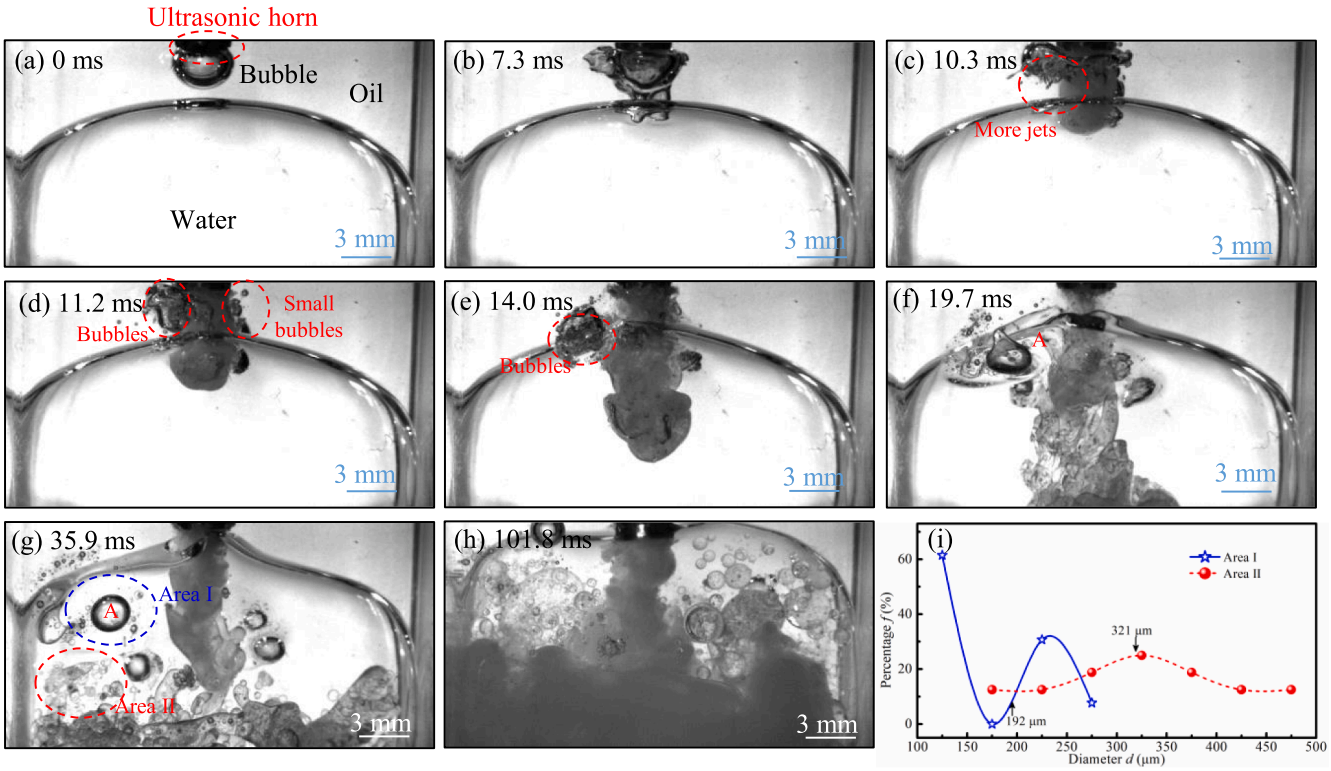

Fig. 4. Effect of a bubble beneath the ultrasonic horn on emulsification: (a)-(h) real-time observation of USE; (f) averaged droplets diameters in Areas I and II. The supplementary video can be accessed with the online version of the article as Video 3.

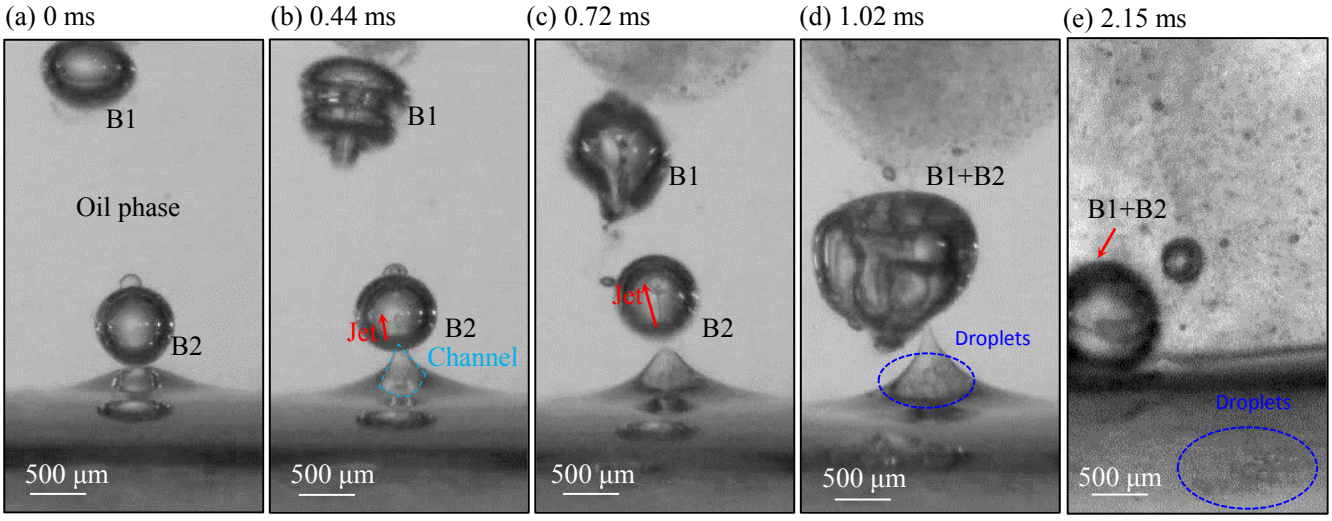

Fig. 5. Interaction of bubble B1 in oil phase and bubble B2 at the interface: (a) 0 ms; (b) 0.44 ms; (c) 0.72 ms; (d) 1.02 ms; (e) 2.15 ms. The supplementary video can be accessed with the online version of the article as Video 4.

(c)). For the very first two to three acoustic cycles the B1 bubble is governed by shape oscillations rather than strong cavitation collapses. This is particularly common in larger bubbles within low surface tension liquids (such as sunflower oil 31–32 mN/m [39]), where the tendency of surface tension to promote sphericity is weaker [24,38]. Shape oscillations are encouraged by anisotropy in the local environment such as the action of the pressure gradient between a compression and the successive rarefaction phase or the appearance of other bubbles in the vicinity (as in this case) that can lead to bubble involution forming a liquid jet in the direction of the acoustic wave propagation [40,41]. Such shape oscillations can break a bubble up, usually generating a small number of fragments as shown in Video 4 (where after the second acoustic cycle a small fragment derived from the tip of the jet is captured). This type of bubble behavior (during the first two acoustic cycles), is described as pancake-to-needle oscillation in Refs. [40,41]. In the successive cycles and until B1 merges with the B2 bubble the behavior of the former is governed by chaotic oscillations.

While bubble B2 gradually rises and eventually coalesces with oscillating bubble B1 in Fig. 5(b)-(d), the combined bubble in Fig. 5(d) gradually sinks due to the primary Bjerknes force, like the bubble in Fig. 2, but keeps chaotic oscillation near the interface. Finally, the formed droplets are pushed back into the water phase by acoustic

streaming, as shown in Fig. 5(e). Hence, the attraction of the bubble at the interface to a bubble in the oil phase not only changes its movement direction (going upwards instead of downwards as in Fig. 2), but also generates more O/W droplet sites at the interface.

3.1.3. A bubble in the water phase away from the interface

Gas bubbles can also be found in the water phase. An example of such bubbles is shown in Fig. 6(a) and (b). Fig. 6(c) presents the interaction of a gas bubble with four oil droplets (D1-D4), that have been formed in water during earlier time steps of USE. As the gas bubble is away from the cavitation region, it does not implode but rather oscillates in a stable fashion. When droplets D1 and D2 come in contact with the bubble in Fig. 6(c_2), they transform from spheres to ellipsoids. After touching the bubble, D1 and D2 seemingly disappear in Fig. 6(c_3) and (c_4). Although the interaction between the bubble and the two droplets cannot be observed in detail, a blurry cluster of small droplets is generated near the bubble as shown in Fig. 6(c_4) and (c_5), which indicates that the initial droplets have been split into smaller ones by bubble vigorous oscillation. Meanwhile, droplets D3 and D4 pass through the bubble top. It is apparent that droplet D4 becomes finer by bubble oscillation, with the diameter decreasing from 185 to 101 μm. Supplementary Video 5 gives a more clear presentation of the above process. Hence, these observations suggest that gas bubbles in the water phase can break nearby oil droplets into finer ones by oscillation.

According to the research of Cucheval and Chow [29], the cavitation zone, which is usually located near the sonotrode, is responsible for the acoustic emulsification of oil, due to micro-jets and shock waves induced by cavitation bubbles collapse. However, it can be found from Fig. 6(a) and (b) that the bubbles far away from the transient cavitation zone can also break up oil droplets into smaller ones, which is a new phenomenon. In this area, gas bubbles keep a stable oscillation, and there are no micro-jets and intensive shock waves, but the dynamic stresses induced by stable oscillation can be in the range 1–500 kPa [30,36]. According to the report of Shanmugam and Ashokkumar [42], in order to enact further disruption of droplets, the shear stress acting on the emulsion droplet has to overcome the Laplace pressure P_L created by the interfacial tension of the fluid. For a spherical droplet with a radius of R, $P_L = 2\gamma/R$, where γ is the interfacial tension. Hence, the Laplace pressure P_L for droplet D4 is 5.4×10^2 Pa (and should be even less for larger droplets like D1), which is significantly lower than the pressure generated by bubble oscillation, thereby showing the potential for the bubbles oscillation to break up the oil droplets.

The observed mechanisms of gas bubbles with different cavitation modes at different locations are schematically depicted in Fig. 7. The different cavitation/oscillation modes of gas bubbles and what conditions should be met to realize the situation have been demonstrated in other researchers' reports [31,36]. For example, if a gas bubble pulsates, implodes and then rebounds and so on, this is called high energy stable cavitation [31]. Hence, the cavitation/oscillation modes of gas bubbles in Fig. 7 could be distinguished clearly by comparing the bubble dynamics in the present paper and other reports [31,36]. When there is a bubble located at the interface of oil and water (Fig. 2), it firstly stably oscillates, as shown in Fig. 7(a). After that, the bubble with a radius larger than the resonance radius ($R > R_{res}$) undergoes high energy stable cavitation [33] (seen in Fig. 7(b)), and sinks gradually into the water phase, accompanied with the oil lining the bubble wall. When the bubble begins to collapse, a part of oil and water beneath the bubble are sucked into the bubble in a form of blended liquid jets, and then they travel through the bubble wall and enter the oil phase, leading to the generation of W/O droplets and O/W/O droplets while the cavitation bubble continues its the implosion journey and eventually splits into smaller bubbles. On the other hand, some oil is pushed into the water phase during the bubble rebound, and then is dispersed to small O/W droplets with the bubble collapse. As for the bubble (Fig. 3) with a radius smaller than the resonance radius ($R < R_{res}$) in Fig. 7(c), it floats up and undergoes low energy stable cavitation [31], leading to the interface instability and the generation of an invert funnel-shaped hump. Due to the drag force, water beneath the interface also floats up and passes through the narrow hump in a form of a small droplet. After that, it keeps to move upwards, and the interface gradually recovers as the bubble is far away from the interface. Comparing the two kinds of bubbles, it can be found that small bubbles move fast and away from the

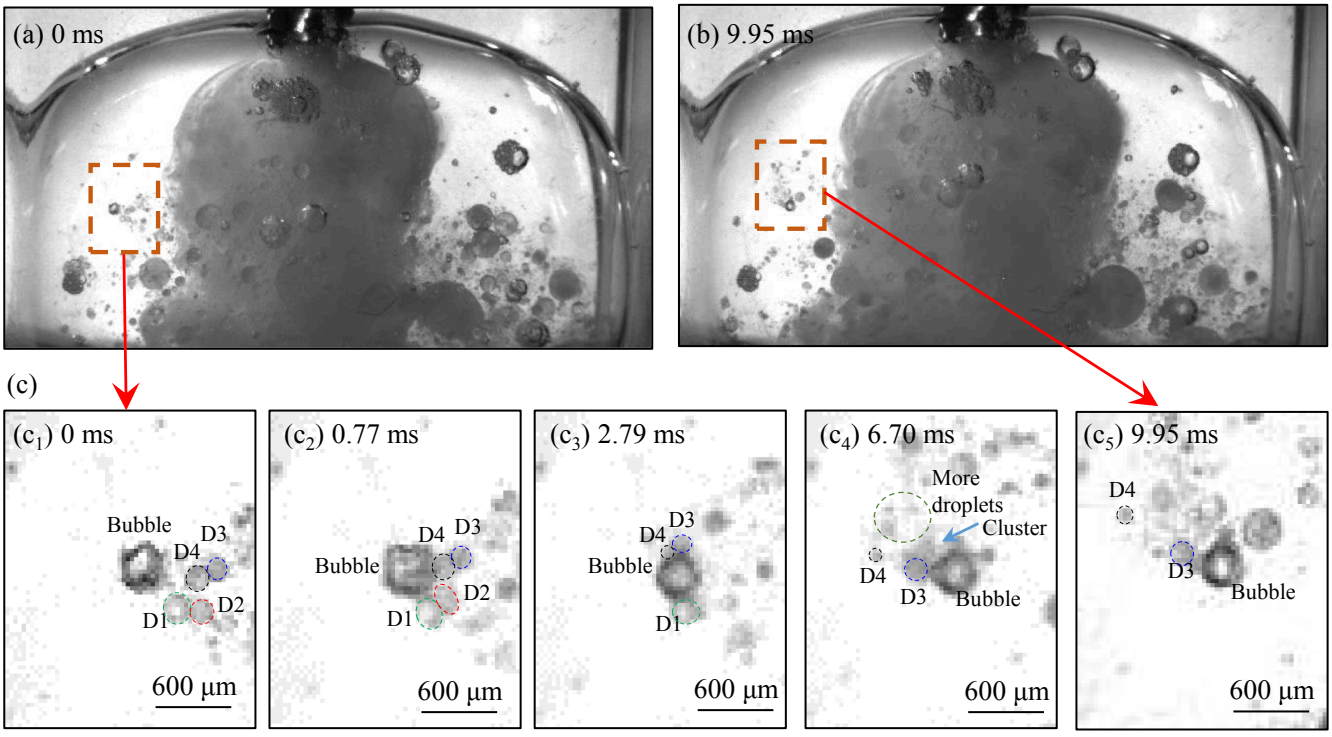

Fig. 6. Ultrasonic emulsification with a bubble in the water phase: (a) initial bubble location in the water phase; (b) bubble location at 9.95 ms; (c) evolution of four droplets interacting with the bubble. The supplementary video can be accessed with the online version of the article as Video 5.

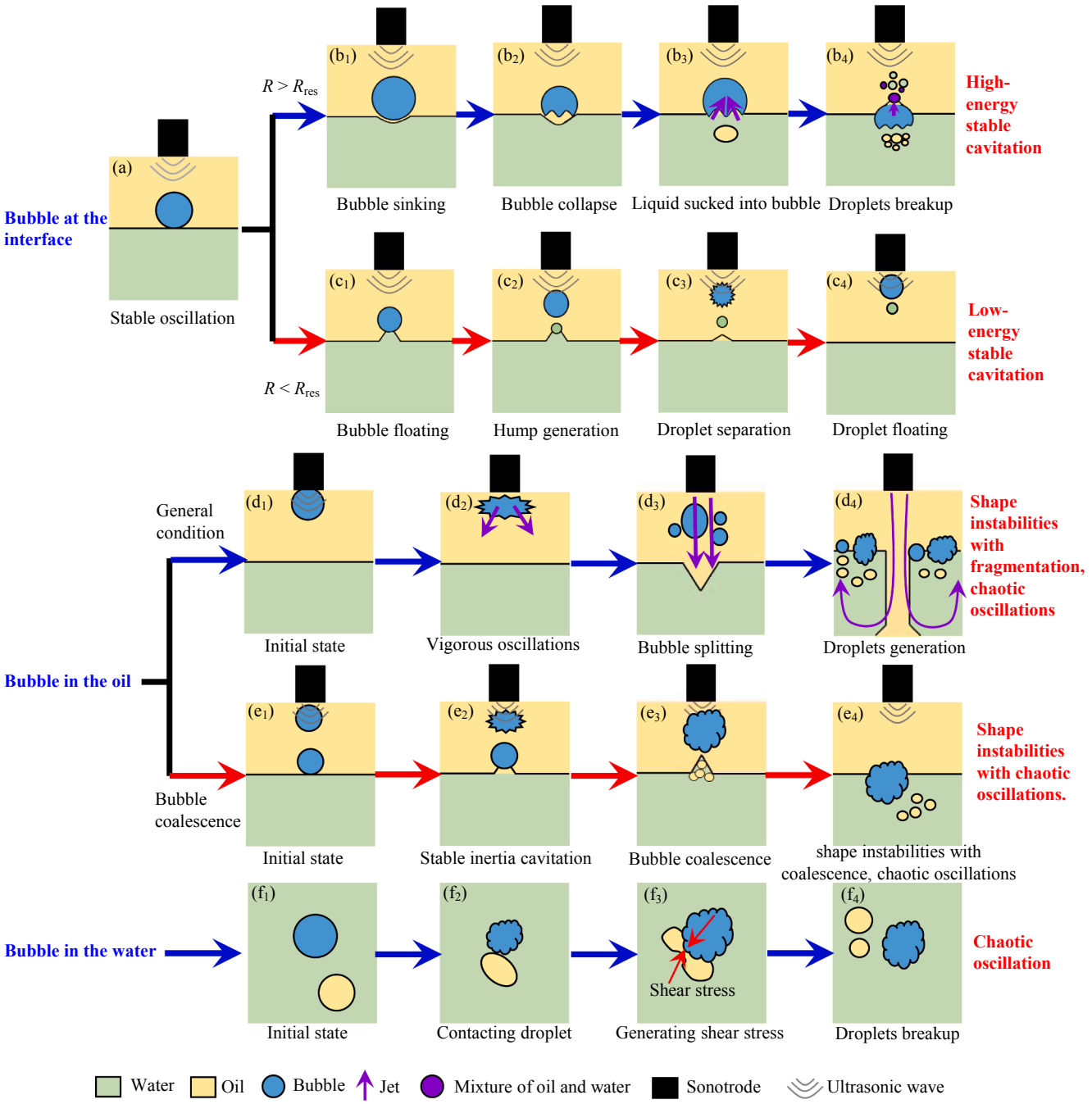

Fig. 7. Schematic diagram of gas bubbles at different locations.

cavitation zone, but big bubbles stay there and play the role of micro-reactors until they collapse, enhancing the mixing of oil and water, so job is done in both cases really, though large bubbles treat more volume and maybe more efficiently. Note that in both cases, the bubble behavior is controlled by the acoustic pressure field as, during this period of time, the interface is always located outside the cavitation zone. By the cavitation zone we understand the active zone where new cavitation bubbles or bubbly clouds are formed, while the observed effects are related to the behavior of pre-existing gas bubbles under the sound wave.

For a large gas bubble near the sonotrode (as shown in Figs. 4 and 7 (d)) and within the cavitation zone, vigorous shape oscillations and splitting into multiple smaller bubbles (bubble fragmentation as previously explained for Fig. 5) occurs. By the action of acoustic streaming, these bubbles move towards the interface undergoing chaotic oscillations [33,36]. During the expansion and contraction of bubbles, oil droplets are pushed into the water phase. A special condition (see Fig. 5) is when there is another bubble in the vicinity as illustrated in Fig. 7(e). Due to the second Bjerknes forces, the upper bubble undergoes repetitive shape oscillations during the very first acoustic cycles with formation of liquid jets and then attracts the lower bubble to float up, forming a bigger bubble with chaotic oscillations. Meanwhile, there is a hump formed at the interface, which is similar to Fig. 7(c_1). Oil and water are suddenly sucked into the narrow hump in just 1 ms, inducing many O/W droplets generated.

When a bubble is in the water phase (Fig. 6), it undergoes chaotic oscillation [33,36] as it is far away from the cavitation zone. If there is an oil droplet contacting the bubble (as shown in Fig. 7(f)), the shear stresses and dynamic pressures exerted by the chaotic oscillation can break the droplet into smaller fragments.

Although the behavior of gas bubbles at the interface (as shown in Figs. 2 and 7(b)) looks similar to that reported for the droplets in an ultrasonic bath by Perdih et al. [18], the principal difference is that the mechanisms observed in our paper and depicted in Figs. 4-6 are rather new and to the best of our knowledge, have not been reported before. Moreover, while Orthaber at al. [28] reports that a bubble initiated inside a denser liquid, e.g. water, generates jets away from the interface, impeding emulsification; our in-situ observation results indicate that gas bubbles with chaotic oscillations in the water phase can enhance the emulsification process. Moreover, it is the first time when the role of gas bubble size, location and interaction with the liquid/liquid interface and droplets is revealed in the USE processing.

These new insights to the mechanisms of gas bubbles in emulsion preparation are beneficial for the optimization of USE process in industry.

3.2. USE of oil–water with different gas concentrations

From the results and analysis given in the previous Sections, it is apparent that the interaction between gas bubbles (long survived and sustained in a cavitating mode) and immiscible liquids is rather complex and there are various mechanisms involved. It is then logical to suggest that the amount of gas bubbles should play a role in emulsification. In order to investigate this hypothesis, two kinds of emulsions were prepared by using water with different gas concentrations as explained in Section 2. The amount of gas concentration is ~ 300 times higher in the commercial carbonated water than that the distilled water. The results in Fig. 8 indicate that USE in the carbonated water produces finer and denser O/W droplets after USE, with these features remaining stable throughout the first day after processing. In both emulsions, droplets coarsen with time, but the diameter of emulsion droplets formed in the carbonated water shows more dimensional stability in time. It should be noted that some big droplets with diameters larger than 100 μm remain stable in the water rather than rapidly rising to the water free surface at the 8th day, as shown in Fig. 8(a_3). The reason is that surfactant (Tween-80) molecules absorbed at droplet surfaces can prevent spontaneous coalescence of these oil droplets, causing the droplets to repel each other.

The quantitative analysis of the obtained emulsions is given in Fig. 9. The average droplet diameter formed upon USE with the carbonated water is 3.0 ± 1.3 μm, which is almost three-fold decrease from that generated by the distilled water, 8.8 ± 4.7 μm. All droplets in the carbonated water range in diameter from 0 to 10 μm, and 95% of them are smaller than 5 μm, which is much more uniform than the size distribution in the distilled water, as presented in Fig. 9(a). Fig. 9(b) shows how the average diameter varies with time. Droplets in the two produced emulsions gradually grow to 38 and 28 μm by the 8th holding day in the distilled and carbonated water, respectively, which demonstrates that introducing more gas in the liquid undergoing ultrasonic emulsification can produce finer and more uniform emulsion droplets. Comparing the slopes of the two lines, it can be found that the slope of the carbonated water is 3.1 μm/day, which is lower than that of the distilled water, 3.9 μm/day. Hence, increasing gas concentration in the emulsion can improve the stability of emulsion droplets.

With considering the in-situ observation results, it can be found that all the cavitation modes play their role in emulsification process. Specifically, it is shown that large bubbles (larger than the resonance radius) near the O/W interface can play the role of a micro-reactor whereupon aggressive implosion (transient cavitation) leads to a fine mixture of water/oil phases. Bubbles at the O/W interface with smaller than the resonance radius tend to continuously oscillate (stable cavitation) dragging droplets in the vicinity of their wakes. Finally, bubbles mainly located outside the cavitation zone, tend to chaotically oscillate under the influence of the acoustic field. However, it should be noted that in the majority of the cases (Figs. 4-6) the chaotic oscillations dominate the observed emulsification mechanisms. Under this regime, cavitating gas bubbles can drag one phase into the other phase, and break up droplets to smaller sizes. Hence, by increasing the gas concentration in the emulsion, even though previous studies have shown that the attenuation of the acoustic wave may increase [43,44], the USE conditions favor chaotic oscillation of gas bubbles [24], which facilitates formation of finer and more stable emulsion droplets.

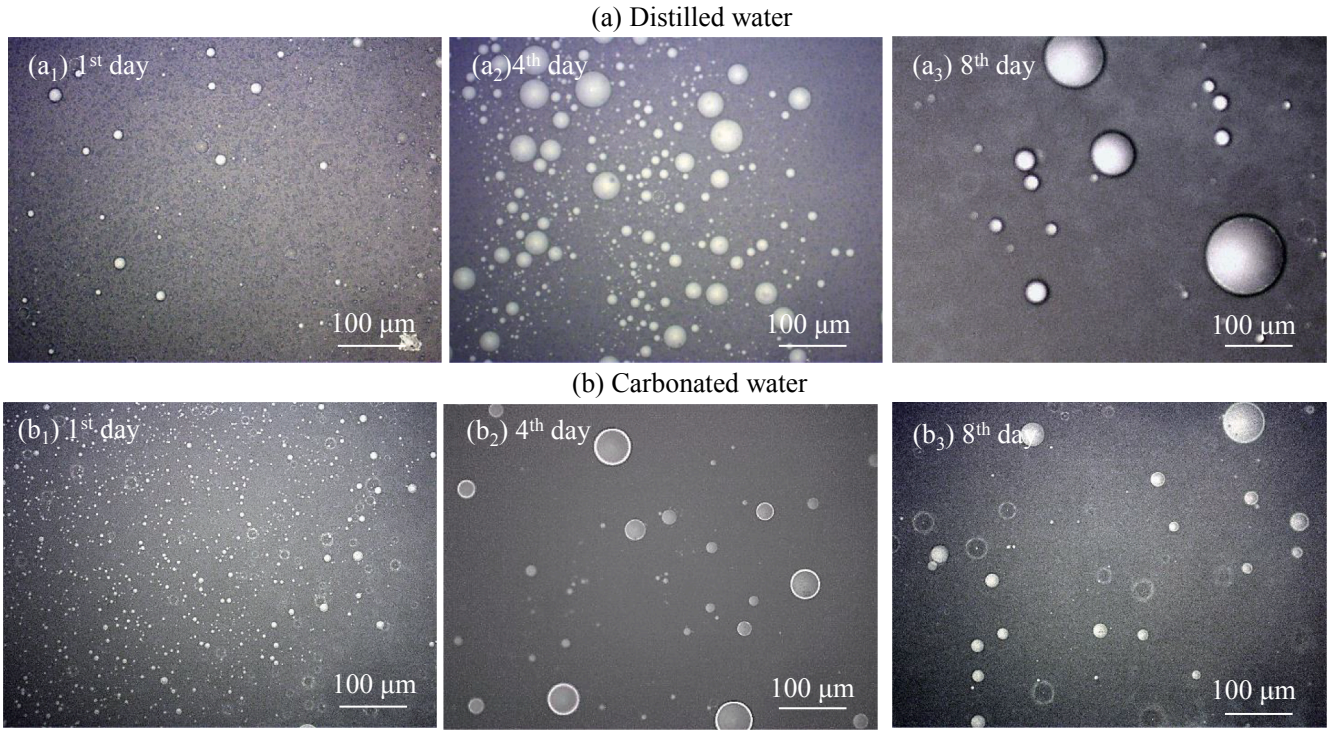

Fig. 8. Emulsion droplets after ultrasonic processing: (a) distilled water; (b) carbonated water.

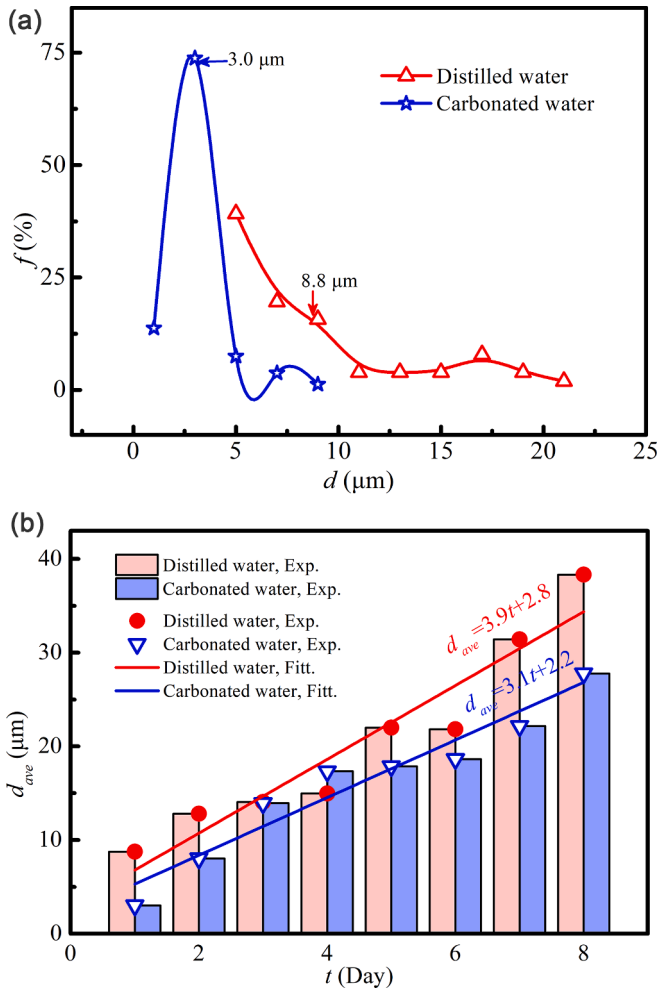

Fig. 9. Quantitative analysis of USE-produced emulsions with different initial concentration of gas: (a) droplet diameter distribution at the 1st day after USE; (b) variation of the average droplet diameter with the holding time.

4. Conclusions

In the present work, a high-speed camera was utilized to capture in real-time the process of interaction of gas bubbles with the oil and water phases during USE. A number of different and new emulsification mechanisms were identified. The effect of gas concentration on the efficiency of USE was quantified through the droplet size distribution and the stability of the droplet sizes. The main results are summarized as follows:

(1) Under the action of the propagating ultrasonic waves, bubbles with a radius larger than the resonance radius located at the interface of oil and water collapse, and penetrate into the water phase dragging oil with it, and thus producing many oil droplets in water beneath the interface. Meanwhile, oil and water are sucked into the imploding bubbles and then disperse water and oil-in-water droplets in the oil phase. Bubbles with a radius smaller than the resonance radius move upwards in the oil phase, leading to small droplets extracted from the water phase and rising up with the bubble.

(2) Large bubbles undergo vigorous repetitive oscillations in the oil phase, and then split into smaller bubbles which is governed by chaotic oscillations. They pass through the interface, and then drag oil into water phase, thereby forming finer O/W droplets than those generated by acoustic streaming.

(3) Gas bubbles in the water phase, farther from the ultrasonic source, undergo violent (chaotic) oscillations, which can fragment nearby emulsion droplets, possibly due to the exerted shear stresses and dynamic pressures.

(4) The chaotic oscillation of gas bubbles is the governing cavitation mode. Hence, with the increase of the gas concentration in an immiscible system, there are more oscillation sites that promote emulsification, leading to the generation of smaller and more stable emulsion droplets.

CRediT authorship contribution statement

W.H. Wu: Methodology, Software, Resources, Validation, Formal analysis, Investigation, Visualization, Writing - original draft. **D.G. Eskin:** Conceptualization, Methodology, Resources, Supervision, Funding acquisition. **A. Priyadarshi:** Methodology, Software, Resources, Investigation. **T. Subroto:** Methodology, Investigation. **I. Tzanakis:** Resources, Funding acquisition. **W. Zhai:** Resources, Funding acquisition.

Declaration of Competing Interest

The authors declare that they have no known competing financial interests or personal relationships that could have appeared to influence the work reported in this paper.

Acknowledgements

This work was financially supported by National Natural Science Foundation of China (Grant Nos. 51922089), and the Engineering and Physical Sciences Research Council of the United Kingdom under UltraMelt2 project (Grant Nos EP/R011001/1, EP/R011044/1 and EP/R011095/1).

Appendix A. Supplementary data

Supplementary data to this article can be found online at https://doi.org/10.1016/j.ultsonch.2021.105501.

References

[1] S.G. Gaikwad, A.B. Pandit, Ultrasound emulsification: effect of ultrasonic and physicochemical properties on dispersed phase volume and droplet size, Ultrason. Sonochem. 15 (2008) 554–563.
[2] J.P. Canselier, H. Delmas, A.M. Wilhelm, B. Abismaïl, Ultrasound emulsification - An overview, J. Dispers. Sci. Technol. 23 (1-3) (2002) 333–349.
[3] K.C.G. Silva, A.C.K. Sato, Sonication technique to produce emulsions: The impact of ultrasonic power and gelatin concentration, Ultrason. Sonochem. 52 (2019) 286–293.
[4] L. Salvia-Trujillo, A. Rojas-Graü, R. Soliva-Fortuny, O. Martín-Belloso, Physicochemical Characterization of Lemongrass Essential Oil-Alginate Nanoemulsions: Effect of Ultrasound Processing Parameters, Food Bioprocess Technol. 6 (9) (2013) 2439–2446.
[5] A.M. Hashtjin, S. Abbasi, Optimization of ultrasonic emulsification conditions for the production of orange peel essential oil nanoemulsions, J. Food Sci. Technol. 52 (5) (2015) 2679–2689.
[6] S. Mohamadi Saani, J. Abdolalizadeh, S. Zeinali Heris, Ultrasonic/sonochemical synthesis and evaluation of nanostructured oil in water emulsions for topical delivery of protein drugs, Ultrason. Sonochem. 55 (2019) 86–95.
[7] S. Mahdi Jafari, Y. He, B. Bhandari, Nano-emulsion production by sonication and microfluidization - A comparison, Int. J. Food Prop. 9 (3) (2006) 475–485.
[8] S. Schultz, G. Wagner, K. Urban, J. Ulrich, High-pressure homogenization as a process for emulsion formation, Chem. Eng. Technol. 27 (4) (2004) 361–368.
[9] S. Sumitomo, M. Ueta, M.A. Uddin, Y. Kato, Comparison of oil-in-water emulsion between ultrasonic irradiation and mechanical stirring, Chem. Eng. Technol. 42 (2) (2019) 381–387.
[10] S.M. Jafari, Y. He, B. Bhandari, Production of sub-micron emulsions by ultrasound and microfluidization techniques, J. Food Eng. 82 (4) (2007) 478–488.
[11] S.A. Neduzhii, On the character of disturbances causing the formation of the emulsion dispersion phase in an acoustic field, Akust. Zh. 10 (1964) 456–464.
[12] M.K. Li, H.S. Fogler, Acoustic emulsification. Part 1. The instability of the oil-water interface to form the initial droplets, J. Fluid Mech. 88 (3) (1978) 499–511.

[13] M.K. Li, H.S. Fogler, Acoustic emulsification. Part 2. Breakup of the large primary oil droplets in a water medium, J. Fluid Mech. 88 (3) (1978) 513–528.
[14] W.H. Wu, W. Zhai, H.B. Hu, B. Wei, Acoustic field and convection pattern within liquid material during ultrasonic processing, Acta Phys. Sin. 66 (2017), 194303.
[15] D.G. Eskin, I. Tzanakis, F. Wang, G.S.B. Lebon, T. Subroto, K. Pericleous, J. Mi, Fundamental studies of ultrasonic melt processing, Ultrason. Sonochem. 52 (2019) 455–467.
[16] W.H. Wu, P.F. Yang, W. Zhai, B.B. Wei, Oscillation and migration of bubbles within ultrasonic field, Chin. Phys. Lett. 36 (2019), 084302.
[17] I. Tzanakis, D.G. Eskin, A. Georgoulas, D.K. Fytanidis, Incubation pit analysis and calculation of the hydrodynamic impact pressure from the implosion of an acoustic cavitation bubble, Ultrason. Sonochem. 21 (2) (2014) 866–878.
[18] T. Stepišnik Perdih, M. Zupanc, M. Dular, Revision of the mechanisms behind oil-water (O / W) emulsion preparation by ultrasound and cavitation, Ultrason. Sonochem. 51 (2019) 298–304.
[19] T.S.H. Leong, T.J. Wooster, S.E. Kentish, M. Ashokkumar, Minimising oil droplet size using ultrasonic emulsification, Ultrason. Sonochem. 16 (6) (2009) 721–727.
[20] N. Vankova, S. Tcholakova, N.D. Denkov, I.B. Ivanov, V.D. Vulchev, T. Danner, Emulsification in turbulent flow - 1. Mean and maximum drop diameters in inertial and viscous regimes, J. Colloid Interface Sci. 312 (2) (2007) 363–380.
[21] W. Lauterborn, C.-D. Ohl, Cavitation bubble dynamics, Ultrason. Sonochem. 4 (2) (1997) 65–75.
[22] O. Behrend, H. Schubert, Influence of hydrostatic pressure and gas content on continuous ultrasound emulsification, Ultrason. Sonochem. 8 (3) (2001) 271–276.
[23] J. Rooze, E.V. Rebrov, J.C. Schouten, J.T.F. Keurentjes, Dissolved gas and ultrasonic cavitation – A review, Ultrason. Sonochem. 20 (1) (2013) 1–11.
[24] I. Tzanakis, G.S.B. Lebon, D.G. Eskin, K.A. Pericleous, Characterizing the cavitation development and acoustic spectrum in various liquids, Ultrason. Sonochem. 34 (2017) 651–662.
[25] F. Chen, C. Dong, C. Chen, W.D. Yin, W. Zhai, X.Y. Ma, B. Wei, Nitrogen-aeration tuned ultrasonic synthesis of SiO2@PNIPAm nanoparticles and preparation of temperature responsive Pickering emulsion, Ultrason. Sonochem. 58 (2019) 104705, https://doi.org/10.1016/j.ultsonch.2019.104705.
[26] O. Behrend, K. Ax, H. Schubert, Influence of continuous phase viscosity on emulsification by ultrasound, Ultrason. Sonochem. 7 (2) (2000) 77–85.
[27] J.J. John, S. Kuhn, L. Braeken, T. Van Gerven, Effect of fluid properties on ultrasound assisted liquid-liquid extraction in a microchannel, Ultrason. Sonochem. 42 (2018) 68–75.
[28] U. Orthaber, J. Zevnik, R. Petkovsek, M. Dular, Cavitation bubble collapse in a vicinity of a liquid-liquid interface - Basic research into emulsification process, Ultrason. Sonochem. 68 (2020), 105224.
[29] A. Cucheval, R.C.Y. Chow, A study on the emulsification of oil by power ultrasound, Ultrason. Sonochem. 15 (5) (2008) 916–920.
[30] Q. Zeng, S.R. Gonzalez-Avila, R. Dijkink, P. Koukouvinis, M. Gavaises, C.-D. Ohl, Wall shear stress from jetting cavitation bubbles, J. Fluid Mech. 846 (2018) 341–355.
[31] T.G. Leighton, The Acoustic Bubble, Academic Press, London, 1994.
[32] H. Search, C. Journals, A. Contact, M. Iopscience, I.P. Address, Quenching mechanism of multibubble sonoluminescence at excessive sound pressure, Jpn. J. Appl. Phys. 40 (2008) 3856–3860.
[33] K. Yasui, Acoustic Cavitation and Bubble Dynamics, Springer, 2018.
[34] Z. Jun, Z. Yuanchun, C. Zhijie, H. Hongzhou, Y. Shaohui, Coalescence dynamic analysis of water droplets in oil in electric field, Trans. Chinese Soc. Agric. Eng. 32 (2016) 284–289.
[35] O. Gmach, A. Bertsch, C. Bilke-krause, U. Kulozik, Impact of oil type and pH value on oil-in-water emulsions stabilized by egg yolk granules, Colloids Surfaces A. 581 (2019), 123788.
[36] T.-H. Kim, H.-Y. Kim, Disruptive bubble behaviour leading to microstructure damage in an ultrasonic field, J. Fluid Mech. 750 (2014) 355–371.
[37] R. Mettin, I. Akhatov, U. Parlitz, C.D. Ohl, W. Lauterborn, Bjerknes forces between small cavitation bubbles in a strong acoustic held, Phys. Rev. E. 56 (1997) 2924–2931.
[38] I. Tzanakis, M. Hadfield, I. Henshaw, Observations of acoustically generated cavitation bubbles within typical fluids applied to a scroll expander lubrication system, Exp. Therm. Fluid Sci. 35 (8) (2011) 1544–1554.
[39] B. Esteban, J.-R. Riba, G. Baquero, R. Puig, A. Rius, Characterization of the surface tension of vegetable oils to be used as fuel in diesel engines, Fuel 102 (2012) 231–238.
[40] T.G. Leighton, An introduction to acoustic cavitation, in: F.A. Duck, A.C. Baker, H. C. Starritt (Eds.), Ultrasound in Medicine, Institute of Physics Publishing, London, 1998, pp. 199–223.
[41] S. Cleve, C. Inserra, P. Prentice, Contrast agent microbubble jetting during initial interaction with 200-kHz focused ultrasound, Ultrasound Med. Biol. 45 (2019) 3075–3080.
[42] A. Shanmugam, M. Ashokkumar, Ultrasonic Preparation of Food Emulsions, Springer, 2017.
[43] I. Tzanakis, G.S.B. Lebon, D.G. Eskin, K.A. Pericleous, Characterisation of the ultrasonic acoustic spectrum and pressure field in aluminium melt with an advanced cavitometer, J. Mater. Process Tech. 229 (2016) 582–586.
[44] I. Tzanakis, M. Hodnett, G.S.B. Lebon, N. Dezhkunov, D.G. Eskin, Calibration and performance assessment of an innovative high-temperature cavitometer, Sensor. Actuat. A-Phys. 240 (2016) 57–69.